Eur. Phys. J. B **48**, 519–528 (2005)
DOI: 10.1140/epjb/e2006-00001-9

THE EUROPEAN PHYSICAL JOURNAL B

Nonlinear dynamics for magnetic systems with a single-spin potential with variable shapes

J.-P. Nguenang[1,2,3,4,a], A. Kenfack-Jiotsa[1,4], and T.C. Kofané[1,4]

[1] The Abdus Salam International Centre for Theoretical Physics, P.O. Box 506, Strada Costiera, 34014 Trieste, Italy
[2] Laboratoire de Physique, École Normale Supérieure de Lyon 46, Allée d'Italie, 69364 Lyon Cedex 07, France
[3] Condensed Matter Laboratory, Department of Physics, Faculty of Science, University of Douala, P.O. Box 24157, Douala, Cameroon
[4] Laboratoire de Mécanique, Faculté des Sciences, Université de Yaoundé I, B.P 812, Yaoundé, Cameroun

Received 8 December 2004 / Received in final form 15 October 2005
Published online 19 January 2006 –

Abstract. Results of computer simulations to investigate the spin dynamics of a classical ferromagnet subject to easy-plane anisotropy and a parameterized Zeeman energy are reported. The variability of the Zeeman term induces a deformable substrate potential in the system. The results show substantial deviations between the conventional sine-Gordon and deformable sine-Gordon description. Solitary-like solutions, shock waves, nanopteron waves and a variety of phenomena, including large easy-plane deviations are also observed. The results display ballistic, diffusive as well as stochastic behaviors. The region of parameters and limits of applicability of deformability effects induced by parameterization of the Zeeman energy are examined.

PACS. 62.30.+d Mechanical and elastic waves; vibrations – 63.20.-e Phonons in crystal lattices – 62.60.+v Acoustical properties of liquids

1 Introduction

The studies of magnetic chains are based upon the existence of beautiful experimental results for neutron scattering in quasi one-dimensional (1D) systems [1–7], and on detailed theoretical work using a variety of methods [8–10]. However, even the extensive investigations that followed these studies could not overcome complicated situations such as the differences between physical systems and theoretical models for dynamics and thermodynamics of spin structures [11–21]. Further investigations of these spin systems also included dipole–dipole interactions, as well as biquadratic interactions for the rigid chains [22–24], and spin–lattice interactions for the compressible chains [25].

Most of the aforementioned studies show that the part of the symmetry-breaking potential introduced into the system through the Zeeman energy contribution, always leads to sine-Gordon (sG) picture. This approximation has given a qualitative description of solitary excitations in magnetic chains and has stimulated widespread interest in the nonlinear dynamics of quasi 1D magnets.

However, the appealing simplified picture that emerges is not sufficient for a quantitative description. Although the macroscopic quantities yield very clear evidence for the contribution of solitons to the spin dynamics, it is also clear that it is still necessary to include fundamental corrections to the simple sG solitons in order to understand more accurately some experiments. For instance the critical field that has been previously established theoretically has not yet been experimentally verified [26].

Besides well known materials such as $CsNiF_3$ which are modeled with a sG equation, and Fe/Cr(211) which is modeled by a sG equation with an additional harmonic on the sinusoidal potential [27,28], it is possible to find in most of these types of material, the presence of some additional interactions that can lead to the frustration of some internal degrees of freedom, and therefore the determination of their ground state appears to be very far from trivial. From a physical viewpoint, it is important to understand the origin of these nonlinear harmonic generations in terms of the microscopic structure and the influence of various interactions. It is important to stress that several effects such as magnetostriction may also lead to new shapes of the domain wall, that are consequences of new harmonic generation in the substrate potential [29,30].

The crucial question for understanding the dynamics of these materials is: *what are the essential terms that should be included or modified in the Hamiltonian to describe more accurately the nonlinear dynamics of magnetic systems subject to harmonic generations?*

[a] *Permanent address*: Condensed Matter Laboratory, Department of Physics, Faculty of Science, University of Douala, P.O. Box 24157, Douala, Cameroon
e-mail: nguenang@yahoo.com

In this respect, the dependence between the properties of real magnetic chains and the number of harmonics in the potential prompted us to undertake investigation of magnetic systems with higher order harmonics. From a mathematical viewpoint, this generalization can be achieved by considering the resulting potential as a standard Taylor expansion with respect to the in-plane angle φ, which contains cosine terms, leading then to a deformable potential as in the case of nonlinear lattices [31,32].

Recently, Kofané [33] put forward a novel model in which the Hamiltonian was characterized by the nearest neighbor exchange energy, the single ion anisotropy and a parameterized Zeeman energy. However, this parameterized model Hamiltonian was limited since the derivation of the nonlinear equation for the spin dynamics needs a certain constraint i.e. ($S = 1$).

The purpose of the present paper is to provide possible answers to the questions posed above related to the proposed model for the real magnetic systems. We want to show that it is possible to increase the range of the reduced magnetic field for the stability of solitary waves, and also set up new features of spin excitations through investigation of their dynamics.

The material of this paper is organized as follows. In Section 2, we present the model Hamiltonian and derive the discrete equations of motion. The implicit kinks are found as exact solutions in the continuum limit. Section 3 is devoted to numerical studies of the effect of the shape parameter on moving solitary excitations in such a discrete magnetic chain. It is shown that in the presence of deformability effects, the sG description is even more likely to provide a very poor description. This is firstly because, due to the existence of the other soliton branches, the shape parameter can lead to a large abrupt velocity change which cannot account for the sG picture. Secondly, for different values of the shape parameter, the number of non-sG solitary structures will be enhanced or reduced with the appearance of new structures. In Section 4, we give a summary and conclusion.

2 The model

To introduce the model in which a relationship between magnetic domain walls and solitons, as special solutions, can be established, let us consider a magnetic chain with the following Hamiltonian

$$H = -J\sum_i \vec{S}_i\vec{S}_{i+1} + A\sum_i \left(S_i^z\right)^2 + g\mu_B\left(1-\eta B_x\right)^2 B_x S\sum_i \frac{\left(1-S^{-1}S_i^x\right)}{1+\left(\eta B_x\right)^2+2\eta B_x S^{-1}S_i^x}. \quad (2.1)$$

Here, the first term represents the ferromagnetic ($J > 0$) or antiferromagnetic ($J < 0$) Heisenberg exchange interaction between neighboring spin vectors. The quantity S represents the modulus of the atomic spin ($S = \left|\vec{S}_i\right|$ in units of $\hbar$). The index x on the magnetic field component means that the magnetic field is applied along the X axis. The Z axis is the direction of the spin chain and the easy plane is the (XY) plane. The second term in the Hamiltonian (2.1) is the single ion uniaxial anisotropy energy due to the crystalline field. It constrains the spin to lie in a plane perpendicular to the chain axis. A is the uniaxial crystal-field anisotropy parameter. The third term is the parameterized Zeeman energy.

We note that the Hamiltonian of any magnet, ferro or antiferro, classical or quantum, on a rigid or deformable lattice, should be time reversal invariant. In particular, this implies that the Hamiltonian cannot contain odd powers of the spin variables or operators. The Zeeman term, for instance, is linear in S^x but does not break time reversal. This is normal because the presence of an external magnetic field changes the sign with time reversal. In the Hamiltonian (2.1), the principal modification that appears is related to the Zeeman term accounting for the deformability effect. The time reversal symmetry is still unlikely to be broken because the shape parameter used here may depend on the applied magnetic field. Therefore, the whole Hamiltonian would be time reversal invariant.

In equation (2.1), η is a parameter that has the inverse dimension of a magnetic field. It depends on the physical properties of the material and also on temperature or pressure. Notice that in all the remaining text the expression ηB_x, which appears in the last term of the Hamiltonian (2.1) is replaced by the parameter r, i.e. $r = \eta B_x$ which is the shape parameter that varies in the range $-1 < r < 1$ [31,32].

In our model Hamiltonian, the subsequent higher harmonics that would be generated in a single spin potential of the system are due to a complex combination of interactions of various intrinsic properties of the material and the applied magnetic field that cannot be derived from Heisenberg's exchange interaction [34]. Three important limits of the Hamiltonian(2.1) can be obtained for r that tends to 1, –1 and 0, leading to a Hamiltonian of a spin system for an Ising-like or a paramagnetic structure, ferromagnetic behavior and a planar Heisenberg structure, respectively.

In classical notation, we represent the spin field in spherical coordinates $\vec{S}_i(z,t) = S(\cos(\theta_i)\cos(\varphi_i), \cos(\theta_i)\sin(\varphi_i), \sin(\theta_i))$, with angles ranging between $0 \le \theta_i \le \pi$ and $0 \le \varphi_i \le 2\pi$. Then, using the undamped Bloch equations for the spin vectors [33], and after some mathematical combinations, the equations of motions are

$$\frac{\hbar}{JS}\frac{d\varphi_i}{dt}\cos(\theta_i) = \sin(\theta_i)\Big[\cos(\theta_{i+1})\cos(\varphi_{i+1}-\varphi_i) + \cos(\theta_{i-1})\cos(\varphi_{i-1}-\varphi_i)\Big] - \cos(\theta_i)\left[\sin(\theta_{i+1}) + \sin(\theta_{i-1})\right] + \frac{2AS}{J}\cos(\theta_i)\sin(\theta_i) + \frac{g\mu_B B_x}{JS^2}\frac{\left(1-r^2\right)^2\sin(\theta_i)\cos(\varphi_i)}{\left[1+r^2+2r\cos(\theta_i)\cos(\varphi_i)\right]^2} \quad (2.2a)$$

$$\frac{\hbar}{JS}\frac{d\theta_i}{dt} = \cos(\theta_{i+1})\sin(\varphi_{i+1}-\varphi_i) + \cos(\theta_{i-1})\sin(\varphi_{i-1}-\varphi_i) - \frac{g\mu_B B_x}{JS^2}\frac{\left(1-r^2\right)^2\sin(\varphi_i)}{\left[1+r^2+2r\cos(\theta_i)\cos(\varphi_i)\right]^2}. \quad (2.2b)$$

The set of coupled nonlinear differential-difference equations (2.2a) and (2.2b), define the collective excitations for the in-plane angle and the out-of-plane angle of a discrete lattice. Although, the model under study is discrete, it is important to derive the continuum limit because it helps in establishing the analytical calculation of the implicit solutions that will be used as initial conditions for our numerical computation. Using the classical approximation at sufficiently low temperature, i.e. neglecting quantum effects [35], in the continuum limit (where the length scale for rotation $\frac{JS}{g\mu_B B_x} \gg 1$), equations (2.2a) and (2.2b) can be reduced to nonlinear partial differential equations. Next, we introduce the dimensionless quantities a_0 (where is the lattice spacing), $\tau = (\frac{2AS}{\hbar})t$ and $b = \frac{g\mu_B B_x}{2AS}$. At the order if $\frac{\partial}{\partial\zeta'}\frac{\partial}{\partial\tau} \sim \varepsilon(\varepsilon \ll 1)$, $\theta \sim \varepsilon$, and $b \sim \varepsilon^2$ [36], equations (2.2a) and (2.2b) then reduce to

$$\varphi_{\zeta\zeta} - \varphi_{\tau\tau} - b\left(1-r^2\right)^2\frac{\sin\varphi}{\left[1+r^2+2r\cos\varphi\right]^2} = 0 \quad (2.3a)$$

$$\theta = \varphi_\tau \quad (2.3b)$$

where b and r are the two constants needed to specify the time evolution of the spin excitations. Equation (2.3a) is the deformable sG equation. The corresponding Hamiltonian density (with the energy measured in units of JS^2 and length units of the lattice spacing) is given by

$$H = \frac{1}{2}\left\{\left(\frac{\partial\varphi}{\partial\zeta}\right)^2 + \frac{1}{c^2}\left(\frac{\partial\varphi}{\partial\tau}\right)^2\right\} + V_{RP}(\varphi) \quad (2.4a)$$

where V_{RP} is the Remoissenet - Peyrard potential given by

$$V_{RP}(\varphi, r) = (1-r)^2\frac{1-\cos\varphi}{1+r^2+2r\cos\varphi} \quad , \quad |r| < 1. \quad (2.4b)$$

Depending on the shape parameter r, this potential can have various shapes as depicted in Figure 1. Therefore, equation (2.3a) can have solutions in the form of large amplitude travelling waves (kinks), low amplitude linear modes (linear spin wave or magnon) and breathers. This equation also shows that in this approximation the solitary excitations are composed of two families of implicit kink solution with the velocity v given in terms of moving coordinates $\xi = \zeta - v\tau$ which are travelling wave rotations of the spin trough 2π within the easy-plane. The implicit

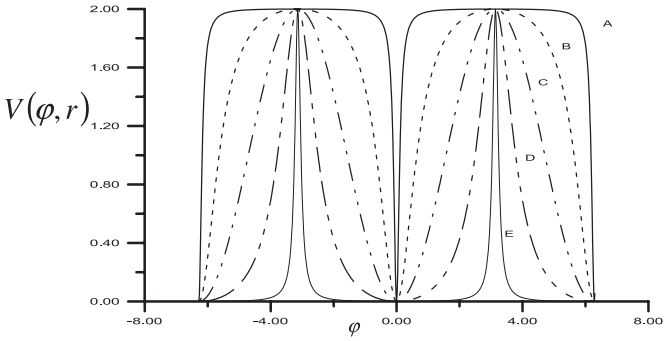

Fig. 1. Schematic plot of the Remoissenet - Peyrard potential for A: $r = -0.9$; B: $r = -0.5$; C: $r = 0$ D: $r = 0.5$; E: $r = 0.9$.

solutions for the in-plane component are [31,32]

$$\frac{\gamma\xi}{d^{(1)}} = \mathrm{sgn}(\varphi-\pi)\left\{\frac{\left(1-\alpha^2\right)^{\frac{1}{2}}}{\alpha} \times \tan^{-1}\left[\frac{\left(1-\alpha^2\right)^{\frac{1}{2}}}{\left(\alpha^2+\tan^2(\varphi/2)\right)^{\frac{1}{2}}}\right] + \tanh^{-1}\left[\frac{\alpha}{\left(\alpha^2+\tan^2(\varphi/2)\right)^{\frac{1}{2}}}\right]\right\}, \quad (2.5a)$$

with the rest energy

$$E_s^{(1)} = 8A'\sqrt{b}\alpha\left(1-\alpha^2\right)^{-\frac{1}{2}}\tan^{-1}\left[\left(\frac{1-\alpha^2}{\alpha}\right)^{\frac{1}{2}}\right] \quad \text{for } -1 < r \le 0 \quad (2.5b)$$

and

$$\frac{\gamma\xi}{d^{(2)}} = \mathrm{sgn}(\pi-\varphi)\left\{\left(1-\alpha^2\right)^{\frac{1}{2}} \times \tanh^{-1}\left[\frac{\left(1-\alpha^2\right)^{\frac{1}{2}}}{\left(1+\alpha^2\tan^2(\varphi/2)\right)^{\frac{1}{2}}}\right] - \tanh^{-1}\left[\frac{1}{\left(1+\alpha^2\tan^2(\varphi/2)\right)^{\frac{1}{2}}}\right]\right\}. \quad (2.5c)$$

And the rest energy is

$$E_s^{(2)} = 8A'\sqrt{b}\alpha\left(1-\alpha^2\right)^{-\frac{1}{2}}\tanh^{-1}\left[\left(\frac{1-\alpha^2}{\alpha}\right)^{\frac{1}{2}}\right] \quad \text{for } 0 \le r < 1 \quad (2.5d)$$

and,

$$\alpha = \frac{1-|r|}{1+|r|}\,; d^{(1)} = d_0\alpha, \quad d^{(2)} = d_0/\alpha; \quad d_0 = 1/\sqrt{b}; A' = \frac{\hbar^2}{2Aa_0} \text{ and } \gamma = \left(1-v^2\right)^{-\frac{1}{2}}. \quad (2.5e)$$

Under this assumption the out-of-plane component, which remains defined by equation (2.3b) for both of the implicit in-plane solutions, indicates that the spin tilting out-of easy plane will be proportional to the kink translation velocity. The in-plane wave rotation component occurs over a characteristic length $d^{(j)}$ $(j = 1, 2)$ which is the "pseudo kink width", determined by the applied field, for velocities v that are expressed here in units of $C_0 = \sqrt{\frac{2AJSa_0^2}{\hbar^2}}$, and the shape parameter r. The antikink solutions are obtained by replacing φ by $(2\pi - \varphi)$. For $r = 0$, equations (2.5a, 2.5c) reduce to the usual sG kink. When r tends to 1, $d^{(2)}$ tends to infinity. On the other hand, when r decreases and tends to –1, $d^{(1)}$ tends to zero. Thus, the kink extension is not only determined by the characteristic length scale d_0, but also by the curvature of the minima. As mentioned above, the deformable sG equation has also the law-amplitude periodic wave solutions of the form $\phi = \phi_0 \cos(q\zeta - \omega_q \tau)$ corresponding to small oscillations of the spin vector around one of the ground states which form a continuous spectrum characterized by the dispersion relation

$$\omega_q^2 = \omega_r^2 + q^2, \quad \omega_r = \left(\frac{1-r}{1+r}\right)\sqrt{b} \tag{2.6}$$

where ω_r is a characteristic frequency of oscillation of an isolated spin vector at the bottom of the substrate potential well ($\phi = 2\pi n$, n integer) and q is the wave vector. The magnitude of ϕ_0 is required to be infinitesimally small, especially in the case where r tends to 1 (see potential with a sharp bottom of Fig. 1E).

3 Numerical calculations

3.1 Computational details

Since the validity of the continuum limit and other approximations, can only be tested by comparison with numerical calculations, we are left with the central question of the physical problem described by the discrete non-integrable system of equations (2.2a) and (2.2b) for our magnetic chain, namely: are the non- linear implicit soliton solutions stable and if so, what is their signature on the dynamics of the magnetic chain for different values of the shape parameter r? For this purpose, our numerical calculations have been achieved on a cyclic chain of 160 spins with periodic boundary conditions and an offset of 2π at chain ends and also with energy conservation imposed. Typically at time $t = 0$, initial profiles are obtained by using the implicit solutions (see Eq. (2.5)). For the numerical implementation of these implicit solutions, instead of the Newton-Raphson scheme (which is just an approximation), we used a different method, which is described below and which turned out to represent a 2π-kink soliton very accurately when $r = 0$. For this purpose, once the velocity v is chosen, next, we define a set of discrete values of the in-plane excitation component such that the interpolation points of lines are given by

$$\varphi_i = \frac{2\pi i}{N} \tag{3.1}$$

with $i \in [0, .., N]$ and $N = 160$ is the spin-lattice size. Using this definition of φ_i in the discrete version of equations (2.5a) and (2.5c) given by:

$$\xi_i = F_1(\varphi_i) \quad \text{for } -1 < r \leq 0 \tag{3.2a}$$

and

$$\xi_i = F_2(\varphi_i) \quad \text{for } 0 \leq r < 1. \tag{3.2b}$$

Here, F_1 and F_2, represent the discrete version of the right hand side of equation (2.5a) and equation (2.5c), respectively. Equation (3.1), equation (3.2a) and equation (3.2b) allow then to recover for each amplitude of φ_i, its corresponding localization on the lattice site ξ_i, for different values of the shape parameter. At this step, we shall reiterate that the out-of-plane component can be defined by the following relationship with the in-plane component:

$$\theta_i = \frac{d\varphi_i}{dt} = -v\frac{d\varphi_i}{d\xi_i}. \tag{3.3a}$$

Therefore, it can be numerically extracted through the following relation

$$\theta_i = -v\frac{\varphi_{i+1} - \varphi_{i-1}}{(\xi_{i+1} - \xi_{i-1})} \tag{3.3b}$$

where v represents the reduced velocity of the solitary excitation in the spin lattice.

In the present simulation, we are able to test the validity of the implicit solutions through their propagation in the discrete chain for different values of the shape parameter r and the reduced magnetic field b. To this end, in our approach, the characterization of both their energy and velocity and the relationship between them are essential in the numerical results, for the first step of such a theoretical study. Such an investigation can serve as a possible basis for the analysis of the energy-momentum curves given by neutron scattering experiments. Needless to say in this discrete model, the parameters $d^{(1)}$ and $d^{(2)}$ that appear in the solution (2.5a) and (2.5c) and defined in equation (2.5e), have the dimensions of length and seem to play the same role as the kink width in the sG system, but this is not exactly the case here. Indeed in the limit $r \to +1$, $d^{(2)}$ diverges as $(1 - |r|)^{-1}$ while the spatial extension becomes infinite; in this case $d^{(2)}$ can be considered as a pseudokink width that will control the effects of discreteness. The parameter $d^{(2)}$ depends not only on the shape parameter r but also on the reduced magnetic field b. So, when this implicit soliton width is large compared to the lattice spacing $d^{(2)} \gg a_0$, the continuum limit is attained in this model and the spin dynamics are mainly dominated by the ballistic behavior. But for negative values of r in the limit$r \to -1$, $d^{(1)}$ tends to zero but the spatial extension of the kink tends to a finite limit. In this case, the continuum limit is no longer controlled by the

parameter $d^{(1)}$. The continuum limit can be attained only if the reduced applied magnetic field is less than $b = 0.3$, with initial velocity in the range $0.02 \leq u_{in}/C_0 \leq 0.5$ i.e. all elements of the ratio $\frac{\gamma}{d^{(1)}}$ need to be taken into account. In this case, the dynamics may display ballistic as well as diffusive behaviors. Let us remember that, in most of the simulations we have chosen the physical parameters so that we avoid a strong discreteness effect. To this end, the implicit static soliton width was kept in a range of 15 to 25 spins during the complete run. We shall address a complete study of discreteness effects and continuum limits in future work.

Let us introduce, as an example, the following set of parameters of the $CsNiF_3$ structure, namely [13]: $J = 23.6$ K, $A = 4.5$ K and $S = 1$. As far as equations (2.2a) and (2.2b) are concerned with the description of the subsequent time evolution of the in-plane and the out-of-plane excitation components, the energy of our discrete magnetic chain is given in a dimensionless form in terms of the in-plane and out-of-plane angle components by $E = \sum_i E_i$, with

$$\begin{aligned} E_i = {} & 1 - \cos(\theta_i)\cos(\theta_{i+1})\cos(\varphi_{i+1} - \varphi_i) \\ & - \sin(\theta_i)\sin(\theta_{i+1}) + 1 - \cos(\theta_i)\cos(\theta_{i-1})\cos(\varphi_{i-1} - \varphi_i) \\ & - \sin(\theta_i)\sin(\theta_{i-1}) + a_2 \frac{\sin^2(\theta_i)}{2} \\ & + a_3(1-r)^2 \frac{1 - \cos(\theta_i)\cos(\varphi_i)}{(1 + r^2, +2r\cos(\theta_i)\cos(\varphi_i))} \end{aligned} \quad (3.4)$$

where $a_2 = \frac{2A}{J}$, $a_3 = \frac{g\mu_B B_x}{JS}$, and the index (i) stands for the lattice sites. With a suitable choice of the time step (typically 0.05 in units $(JS)^{-1}$), this energy, which is a conserved quantity, was frequently monitored in our simulations to ensure an accuracy of about 0.01% for the fourth order Runge–Kutta scheme.

3.2 Numerical results

Let us first present Figure 2 where we plotted the maximal out-of plane spin deviation component as a function of the shape parameter r, while the initial condition is that of the kink soliton of the sG equation for the curve A. The curve B corresponds to the case of the implicit soliton solution as the initial conditions in our numerical scheme. In order to store the data of these curves, we computed, for each value of the shape parameter, the values of the out-of-plane component, and we kept only their maximal values ($\theta_{\max}$) for the reduced magnetic field in the range $0 \leq b \leq 0.61$. These curves show that for the entire range of the shape parameter, the out-of-plane spin tilting is always greater in the case of curve A than that of curve B. Since a system with higher values of the out-of- plane component is more prone to instability, this is thus the proof that the nonlinear excitations are more subject to instability if the initial conditions are the conventional sG-kink solitons than when the implicit solution of the continuum limit are chosen as initial conditions. For this reason, we have chosen the implicit solitons as initial conditions for all the remaining results.

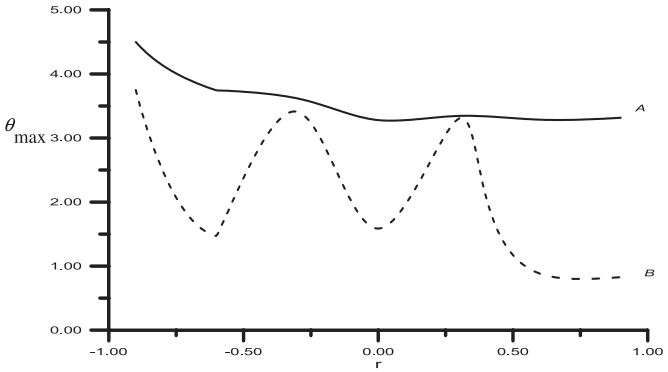

Fig. 2. Plot of the maximum out-of plane angle deviation θ_m from the easy plane as a function of the shape parameter r. A: — Solid line corresponds to the case of sine-Gordon soliton as initial condition. B: - - - Dashed line corresponds to the case of the implicit soliton as initial condition.

The discrete-lattice time evolution requires specification of r, b and the initial velocity u_{in}/C_0. A series of runs were performed holding the shape parameter r fixed but varying the reduced magnetic field b and the velocity of the input implicit solitary excitation (and therefore the energy) u_{in}/C_0. In order to measure the effective velocity of the topological solitary wave of kink type, we started at the beginning of the simulation by identifying at each time step, the centre of the solitary excitation as the point at which the amplitude $\varphi = \pi$. Then, the oscillations in the solitary excitation velocity were averaged numerically over 1500 units of time during which the solitary wave at low magnetic field and high initial speed ($u_{in}/C_0 = 0.7$) could translate approximately 70 unit cells in the course of calculation, and this averaged velocity was identified as the solitary excitation's propagation velocity.

When $r = 0$, and mainly in the range $-0.2 \leq r \leq 0.2$, we found that if the implicit solutions (which in this case should reduce to that of the sG approximation) were valid, then the propagation velocity of the soliton would be that of the initial condition u_{in}/C_0. We found as Wysin, Bishop and Kumar (WBK) [37,38] that, on the contrary, the solitary wave's motion is different at arbitrarily low non-zero velocity and the difference increases with increasing magnetic field. This point is illustrated in Figure 3a where the effective velocity of the solitary excitation is plotted as a function of the input velocity of the initial condition. Our numerical scheme also enables us to obtain the same result as WBK for the energy velocity relationship, where significant deviation from the sG branch [37] is observed as the magnetic field increases. To illustrate this point, we have plotted in Figure 3b the dispersion relation in terms of the energy as a function of the effective velocity of the solitary excitations for different values of the magnetic field, in the case of $r = 0$.

From Figures 3a and 3b, it is clear that the results obtained are qualitatively the same as those obtained previously by WBK in reference [38] while investigating the

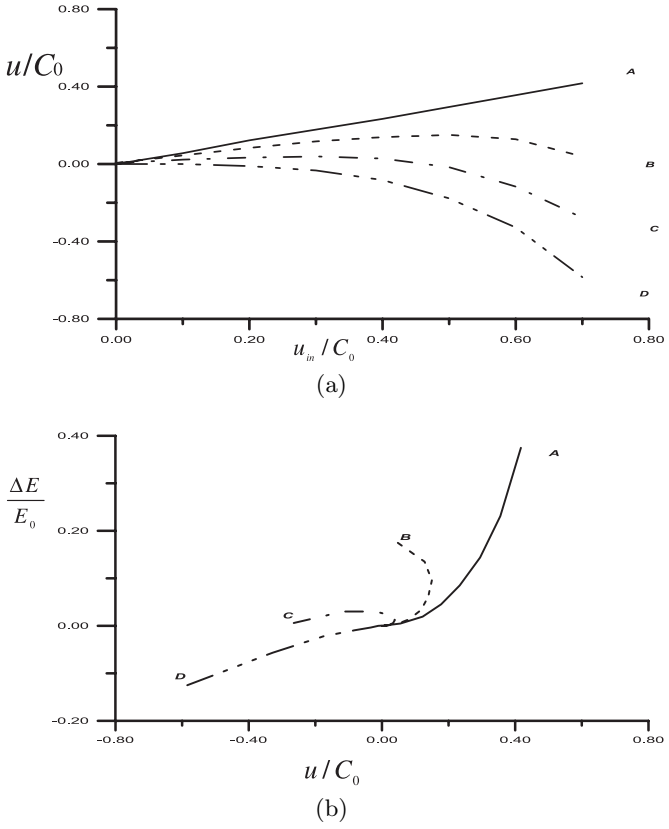

Fig. 3. (a) Plot of the numerical computation of the mean soliton velocity u/C_0 as a function of the implicit deformable sine-Gordon kink initial conditionu_{in}/C_0 when r=0 for some values of the reduced magnetic field b: A: 0.05; B: 0.15; C: 0.25; D: 0.35. (b) Plot of the energy $\Delta E/E_0$ velocity relation for the soliton-like excitation in a ferromagnetic chain when the deformability effects are absent i.e. $r = 0$. The curves in (b) that take the following values: A, 0 (full curve); B, 0.15 (broken curve); C, 0.25 (chain curve); D, 0.35 (dot-dot-dot dash curve).

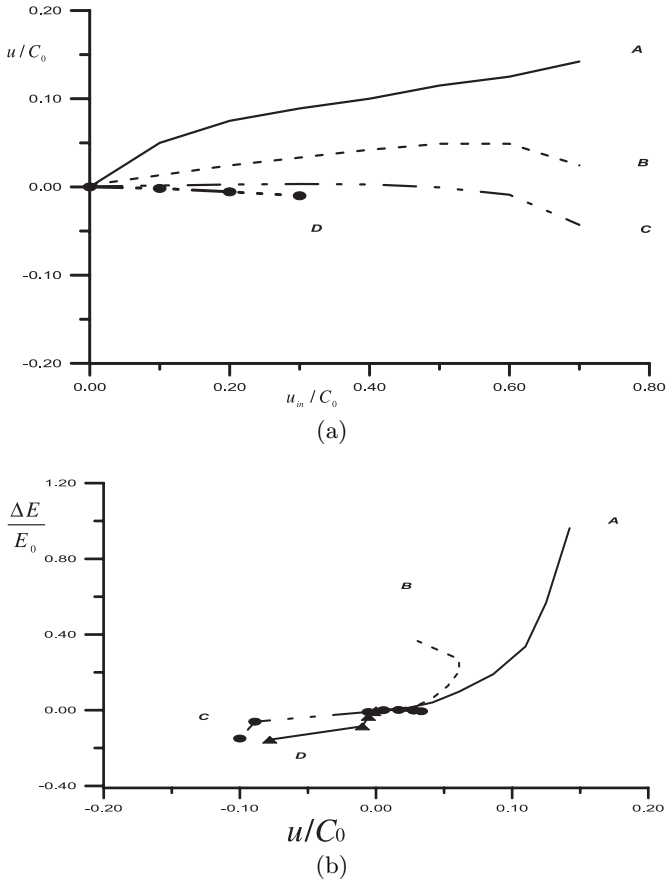

Fig. 4. (a): Plot of the numerical computation of the mean resulting soliton velocity u/C_0 as a function of the implicit deformable sine-Gordon kink initial condition u_{in}/C_0 when $r = -0.8$ for some values of the reduced magnetic field b: A: 0.05; B: 0.22; C: 0.35; D: 0.5. (b) Energy against mean resulting soliton velocity, when $r = -0.8$, for the following values of the reduced magnetic fields b. A: 0.05; B: 0.25; C: 0.35; D: 0.5.

dynamics of a rigid ferromagnetic chain. The only slight difference is related to the small values of the effective velocity of the solitary excitations. This is normal because the implicit solution used here is not a good solution for the system when $r = 0$. Therefore, in absence of deformability effects in the spin chain, we obtained the same results as those of previous studies [37,38], which were concerned with the dynamics of a rigid magnetic chain. It is worth mentioning that these results could be predictable from the result obtained in the case of the Hamiltonian limit when r=0, but it is also useful to derive them with the same approach that we use for $r \neq 0$ in order to validate our numerical method.

When $r \neq 0$, the most interesting behavior is obtained for $r < -0.2$ and $r > 0.2$ and the general features of the deformability effect on the dynamics of a spin chain are illustrated in most of the figures presented below. We shall first focus our attention on the case where $r < -0.2$, and mainly for lower values of r. One of the main effects of the deformability in the system appears in the energy and the effective velocity curves of the solitary excitation, respectively. Figures 4a and 4b, obtained for $r = -0.8$, show the plot of the effective solitary wave velocity against the implicit initial conditions velocity and the total energy against the effective propagating solitary excitation velocity, respectively. In Figure 4a, the curve A corresponds to the case of a solitary excitation propagating when the magnetic field is approximately zero. Increasing the magnetic field, in curve B and C we observe as in curve A an increasing of the effective velocity up to a maximal value after which it starts decreasing. For these curves, the main effect of the deformability occurs in the lowest values of the solitary excitation speeds compared to those of the initial conditions. The effective velocity here is almost lower than in the case of $r = 0$ corresponding to the rigid magnetic chain [37]. This can be understood by the fact that for this value of deformability parameter, and mainly in the range $-1 < r \leq -0.6$, the resulting kink narrows and its profile is very sharp, thus it faces discreteness effects of the spin lattice that tend to lower its velocity. In the case of curve D, we only plotted a few points, because the effective velocity starts by decreasing down to a

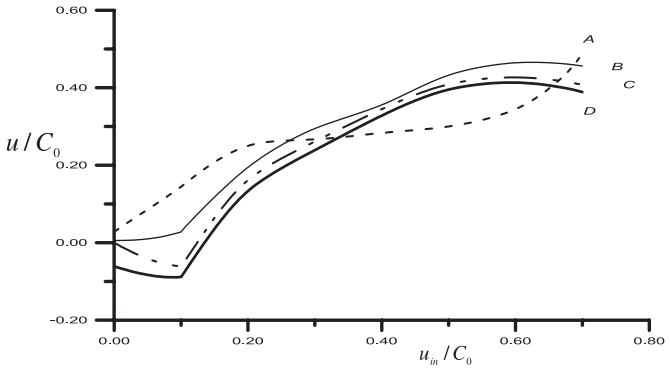

Fig. 5. The same method is applied here as in Figure 5 to obtain the velocity of the resulting solitary excitation u/C_0 as a function of u_{in}/C_0 when $r = 0.9$, for the following values of the reduced magnetic field b; A: 0; B: 0.2; C: 0.3; D: 0.5.

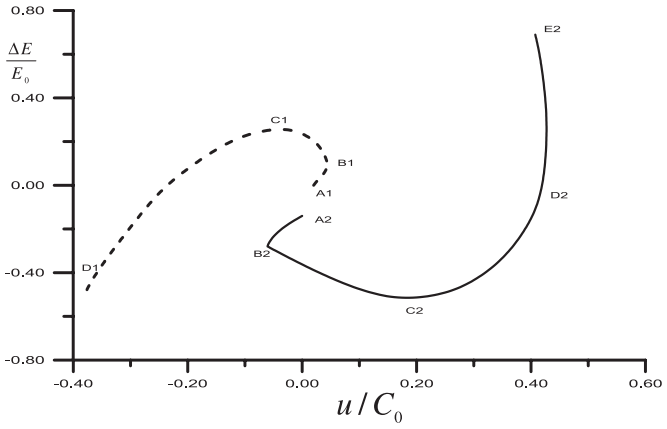

Fig. 6. Plot of the energy $\frac{\Delta E}{E_0}$ velocity relation for the soliton –like excitation in a ferromagnetic chain, when the system is subject to deformability effects for $r = 0.9$ and the reduced magnetic field $b = 0.3$. The curve with dashed line corresponds to the case of the same value of the reduced magnetic field but without deformability effect ($r = 0$ and $b = 0.3$). Here $\Delta E = E(u) - E_0$ where $E_0 = E(u = 0)$ is the rest energy.

certain minimal value. Further increasing the initial velocity leads to an instability of the excitation. This is explained by the fact that, for this largest value of the reduced magnetic field (i.e. $b > 0.3$), when the initial condition is introduced in the chain with a certain initial momentum, the resulting wave is suddenly subject to an interplay between its momentum and an opposite force induced by the complex combination of the magnetic field and the intrinsic properties of the material. Consequently, in this range of deformability parameter and magnetic field, with a higher range of the initial velocity, the solitary excitation suffers strong discreteness effect that finally destroys its shape. In Figure 4b, while looking at the case of curve A and curve B, we can see that even if quantitatively the deformability affects the values of the energy, qualitatively the system displays behavior close to the result obtained in the case of $r = 0$ in Figure 3b in this parameter range. The implicit initial condition turns out to produce excitations in the chain whose energy displays less than three regimes as the reduced magnetic field increases up to a value of $b = 0.25$. Increasing the value of the reduced magnetic field further led the system to unstable behavior in the energy and velocity relationship. Thus the difference matches qualitatively and quantitatively the case of $r = 0$. From these figures it is also clear that, due to the lowest values of the computed velocities compared to those of the initial conditions, the implicit 2π-kink solitary excitations are not valid solutions of the system.

For $r > 0.2$, we can see that the implicit soliton solutions are not valid. This can be seen in the shape of the average soliton velocity obtained in Figure 5. In this figure, the effective soliton velocity plotted as a function of the velocity of the initial condition displays non-equal values for $r = 0.9$. But, for lower values of the magnetic field and lower speed ($u/C_0 \leq 0.2$), the implicit solitons are still valid. For positive values of the shape parameter r, one of the most important features of the deformability effect is illustrated in Figure 6, where the energy is displayed in terms of the ratio $\Delta E/E_0$ as a function of the effective velocity of the solitary excitation both for the case of a planar Heisenberg spin chain ($r = 0$), and a spin chain with deformability effect (see the curves with A2, B2...). Here, and in other cases, $\Delta E = E(u) - E_0$ where $E_0 = E(u = 0)$ is the rest energy of the soliton. The first difference is related to the concavity of the two curves which are opposite. Therefore, another feature of the deformability effect is that it transforms a forward motion of the solitary excitation into a backward motion. The second difference comes from the fact that, although both of the curves have been obtained for the same value of the applied magnetic field (i.e. $b = 0.3$), the second curve displays four excitations branches for $r = 0.9$, while the first curve which is not concerned with deformability effects displays only three excitation branches. Therefore, in this case, the deformability also increases the number of excitation branches. Similar curves symmetric from those presented in this figure can be obtained by changing the sign of the velocity of the implicit initial condition. A numerical result which appears surprising at first glance when looking at Figure 6, is that, from point A2 to B2, the velocity against energy, instead of a single valued behavior, displays coupled energy behaviour. From point A2 to B2, which corresponds to the first branch, the nonlinear excitations, when initiated, suddenly split into a bi-kink that starts a transparent collision process, while propagating in the opposite direction to that of the initial condition. This transparent collision process induces an energy cost that progressively decreases its initial value. This strange behavior comes from a combination of the deformability effect and the magnetic field that act to constrain the magnetic excitation to propagate in the opposite direction. Next, from point B2 to point C2 that corresponds to the second branch, the nonlinear excitation is of a kink type that still loses energy while propagating in the positive direction. Hence, the velocity may then display bi-valued energy behavior in this velocity range. In the third branch (III) that begins from point C2 and ends at point D2, the

soliton energy increases with an increase of its velocity. The energy-velocity relationship along this branch is similar to the one given by the deformable sG(dsG) equation; therefore this branch can be called the dsG-soliton branch. In the branches I, II, and IV significant deviations from dsG soliton behavior can be observed. When one follows the curve from point A2 to E2, the magnitude of the out-of-plane component deviation θ increases from 0 to $\pi/2$. It is therefore enough to cause an instability in the in-plane excitation. Beyond point D2, the localized pulse type excitations which can propagate develop a shock front. Due to the slow decreasing of the effective velocity, new excitations that may behave as a nanopteron-like wave [39] may also propagate. This can be easily understood, when we make a comparison with the results of WBK [37,38] for a rigid magnetic chain, or Roche and Peyrard for a magnetic chain subject to impurity [36].

From Figure 7 that illustrates the magnetic field and the solitary excitation's maximal velocity relationship for six cases (*A:* $r = -0.6$*; B:* $r = -0.3$*; C:* $r = 0$*; D:* $r = 0.3$*; E:* $r = 0.6$*; F:* $r = 0.9$), it is clear that the range of the reduced magnetic field ($0 \leq b \leq 0.61$) for the magnetic chain under deformability effects in which stable non linear excitations can propagate is larger than that of the rigid magnetic chain ($0 \leq b < 0.33$) [12,13,26]. As we can see in this range of the reduced magnetic field when $r \neq 0$, the nonlinear excitation propagates with a non-zero maximal velocity and for positive values of the parameter r, the magnetic field and the solitary excitation's maximum velocity present a semi circular-like behaviour. The non-zero velocity here can be understood as in reference [39] in terms of the absence of a standing bound state in the magnetic chain for each value of the magnetic field considered here, when the solitary excitation reaches with its maximal speed. When $r = 0$, we recover in Figure 7c the Magyari-Thomas [12,16] shape and the critical magnetic field close to $b = 1/3$, which is consistent with their result $B(0) - B(u) \approx u^{2/3}$. The absence of non-static critical magnetic field for the magnetic excitations of a spin chain under deformability effect may also justify the reason why until now the critical magnetic field, although theoretically well established for the rigid magnetic chain, has not yet been found experimentally.

In Figure 8, we plot the energy curve as a function of the magnetic field relationship for five cases (*A:* $r = -0.9$*; B:* $r = -0.6$*; C:* $r = 0$*; D:* $r = 0.6$*; E:* $r = 0.9$). From this figure we notice that, while most of these curves display an expected behavior i.e. the energy curve decreases with increasing the magnetic field, the lowest values attained on this energy curve seem to be nonlinear as the shape parameter increases. This is the proof that in most cases, the solitary excitations retain their shape and do not split into other excitations, even if they do not display equivalent minimum energy. This is due to the different nature of the nonlinear excitations that the system displays when one varies the shape parameter. The most surprising result here is that of curve A, which corresponds to the case of $r = -0.9$. Here, instead of showing a decreasing behaviour, the energy curve displays an increasing one as the magnetic field increases. This can be understood in the sense that, for this value of the shape parameter and mainly in the range $-1 < r \leq -0.9$, the magnetic chain structure changes drastically. This may be the signature of a ferromagnetic chain with non linear excitation energy that is non-conservative. This can be seen as a special feature of the intrinsic damping induced by the deformability effects on the excitations that move in the system within this parameter range. Another feature of the deformability effect is that the energy decreases down to non-vanishing values, which is not the same as in the curve C where deformability is absent. We have illustrated other features of the deformability effects in Figure 9 where the time evolution of the density of energy curve on the lattice sites is represented. We notice that, under deformability effects, the spin dynamics display stochastic behavior for $r = -0.9$ and $b = 0.1$ (curve A), that manifests itself as a combination of an intermittency with a repetition of the trajectory

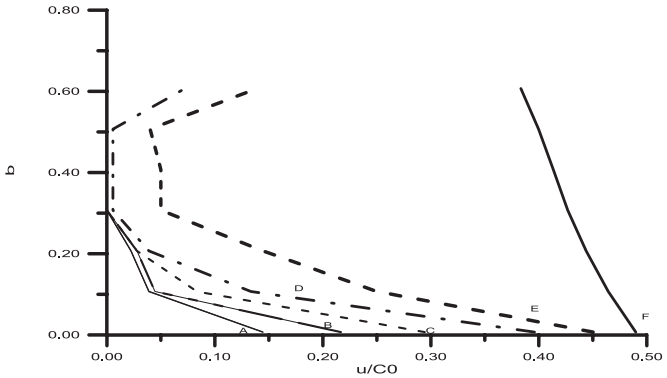

Fig. 7. Maximum mean propagation velocity of the resulting soliton against magnetic field for some values of the deformability parameter A: $r = -0.9$; B: $r = -0.6$; C: $r = 0$; D: $r = 0.6$; E: $r = 0.9$.

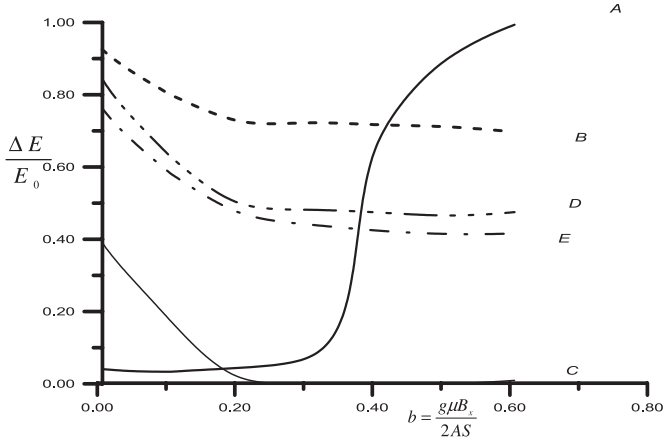

Fig. 8. Energy $\Delta E/E_0$ as a function of the reduced magnetic field b, for some values of the shape parameter A: $r = -0.9$; B: $r = -0.6$; C: $r = 0$; D: $r = 0.6$; E: $r = 0.9$. Here $\Delta E = E(u) - E_0$ with $E_0 = E(u = 0)$. Only the case of curve C ($r = 0$) is typical, all the other curves have been fitted by multiplying ordinate values by 0.01. their greatest values are due to the division in the definition of the energy in equation (3.1).

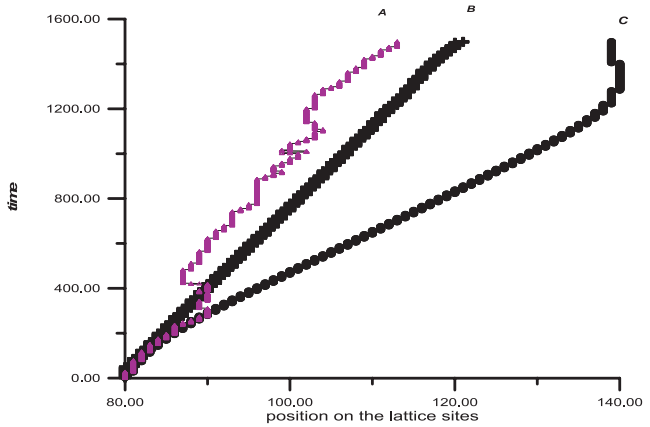

Fig. 9. Energy density along the chain versus time for three values of the shape parameter A: $r = -0.9$. and $b = 0.1$; B: $r = 0.9$ and $b = 0.3$; C: $r = 0.6$ and $b = 0.1$.

of the excitation while moving; and also ballistic behavior for the case of $r = 0.9$, $b = 0.3$ (curve B), and diffusive behavior for $r = 0.6$ and $b = 0.1$ (curve C). Needless to say, these chaotic and diffusive behaviors are due to the fact that the initial conditions used are not the solution of the discrete system. Therefore, when these implicit initial conditions are used, they induced many other excitation modes in the system that do not lead to a ballistic behavior of the solitary excitation. This is different from the result obtained in the case of a rigid magnetic chain (i.e. $r = 0$), for the same values of magnetic field and initial velocity.

4 Summary and conclusion

To summarize, we have introduced phenomenologically nonlinear harmonic generation in the substrate potential through deformability effects, in a model of a one dimensional Heisenberg spin chain where the Zeeman energy is parameterized. Taking into account this deformability effect has led us to a substrate potential in the system for which the energy lost of the solitary excitation is intrinsically considered. Although little is known about the details of this phenomenon in a magnetic chain, we believe that, such effects must be considered to obtain reasonable agreement between experiment and theory.

With this model, we have tested the validity of the implicit solitary solution by numerical computation in a classical easy-plane ferromagnetic chain with a variable substrate potential, for the shape parameter in the range $-1 < r < 1$.

For $-1 < r < 0.2$, as the shape parameter r is decreasing, we observe in certain cases the possibility of an excitation with a velocity that displays three different values of the energy. We also notice that, depending of the range of the reduced magnetic field b, the number of soliton branches may be reduced or enhanced. The system seems to display a stochastic behavior for decreasing values of the shape parameter.

For the range $-0.2 \leq r \leq 0.2$, and different values of the magnetic fields, our results are similar to those of WBK [37,38]. This means that the implicit solitary solutions are valid for lowest branches. The system also displays large easy-plane deviation, temporal oscillation and shock wave formation.

When $r > 0.2$, we observe that even if there appears to be a difference between these curves and the case of $r = 0$, it remains the fact that, there is a difference between the velocity at which we launch the solitary excitation and the observed velocity at any arbitrary low non-zero velocity. This difference increases with increasing magnetic field. We also notice the presence of a non-standing bound state when the nonlinear excitation evolves with its maximal speed. The energy velocity diagram enables the deduction of the presence of four nonlinear excitation branches in which one is new for the particular case of $r = 0.9$ and $b = 0.3$. The new excitation branch is progressively dominated by nanopteron wave formation [39]. From our results, it is clear that the range of the magnetic field for stable non-linear excitations propagating in a magnetic chain under a deformability effect is greater than that of the rigid chain that was inconsistent with experiment [26]. The reason for this enlargement can be understood by the fact that previous theoretical models were too simple to represent real specimens. Very often, if a more realistic model is used, the results become complex enough to have a clear physical interpretation. Therefore, neglecting key effects may lead to misleading theoretical predictions. The ideal system is the one in which the leading physical features are well represented by a simple theoretical model. Thus, one should take care of the range of the shape parameter r chosen when the dynamics and also thermodynamics of such a magnetic chain are studied. Therefore, the conventional sG based on a phenomenological description for the 1D system should be profoundly affected. However, before assessing the consequences of the shape parameter on a 1D system, it is necessary to study the implicit kink-antikink scattering and also the implicit kink-kink like collision, along with an extensive investigation of their impact on the discreteness effects, as well as their competition with the impurity effect in a disordered system. Due also to the multiple propagating behaviors displayed by the findings, and the abrupt change on the energy for a certain range of the shape parameter for a given magnetic field, a study of the induction of a phase transition by implicit solitons in such a 1D magnetic system is encouraged. We shall report our results for these investigations in future work.

Dr. Nguenang Jean-Pierre would like to thank the International Centre For Theoretical Physics (ICTP) and the Swedish International Development Agency (SIDA) for sponsoring his Visit at the ICTP in Trieste where this work was started. He would also like to thank the Agence Universitaire de la Francophonie (AUF) for sponsoring his research stay at the Laboratoire de Physique de l'École Normale Supérieure de Lyon. Helpful suggestion of Prof. Michel Peyrard of Laboratoire de Physique de l'École Normale Supérieure de Lyon in the final version of this paper is greatly appreciated.

References

1. M. Steiner, J. Vilain, C.G. Windsor, Adv. Phys. **25**, 87 (1976)
2. T. Goto, Y. Yamgushi, J. Phys. Soc. Jpn **50**, 2133 (1981)
3. A.P. Ramirez, W.P. Wolf, Phys. Rev. Lett. **49**, 227 (1982)
4. J.P. Boucher, L.P. Regnault, J. Rossat-Mignot, J.P. Renard, J. Bouillot, W.G. Stirling, J. Appl. Phys. **52**, 1956 (1982)
5. F. Borsa, Phys. Rev. B **25**, 3430 (1982); F. Borsa, M.G. Pini, A. Rettori, V. Tognetti, Phys. Rev. B **28**, 5173 (1983)
6. M. Steiner, K. Kakurai, J.K. Kjems, Z. Phys. B **53**, 117 (1983)
7. K. Kopinga, A.M.C. Tinus, W.J.M. de Jonge, Phys. Rev. B **29**, 2868 (1984); A.M.C. Tinus, W.J.M. de Jonge, K. Kopinga, Phys. Rev. B **32**, 3154 (1985)
8. H.J. Mikeska, J. Phys. C **11**, L29 (1978)
9. E. Alltroth, H.J. Mikeska, Z. Phys. B **43**, 209 (1981)
10. C. Etrich, H.J. Mikeska, E. Magyari, H. Thomas, R. Weber, Z. Phys. B **62**, 97 (1985)
11. *Magnetic Excitations and Fluctuations*, edited by S.W. Lovesy, U. Balucani, F. Borsa, V. Tognetti (Springer, Berlin, 1984)
12. E. Magyari, H. Thomas. Phys. Rev. B **25**, 531 (1982)
13. P. Kumar, Phys. Rev. B **25**, 483 (1982); P. Kumar, Physica D, 359 (1982)
14. D. Hackenbraccht, H.G. Schuster, Phys. Rev. B **27**, 572 (1983); D. Hackenbraccht, H.G. Schuster, Phys. Rev. B **27**, 6916 (1983)
15. R. Liebmann, M. Schobinger, D.J. Hackenbracht, J. Phys. C **16**, L633 (1983)
16. E. Magyari, H. Thomas, J. Phys. C **16**, L535 (1983)
17. E. Magyari, H. Thomas, Phys. Rev. Lett. **51**, 54 (1983)
18. H.J. Mikeska, K. Osano, Z. Phys. B-Condensed. Matter **52**, 111 (1983)
19. H.J. Mikeska, Physica B **120**, 235 (1983)
20. P. Kumar, V.K. Samalam, Phys. Rev. Lett. **51**, 54 (1984)
21. H.C. Fogedby, P. Hedegard, A. Svane, Phys. Rev. B **28**, 2893 (1983)
22. J.P. Nguenang, T.C. Kofané, Phys. Scri. **55**, 367 (1997)
23. J.P. Nguenang, T.C. Kofané, E. Yomba, J.D. Yo, Phys. Scr. **60**, 460 (1999)
24. J.P. Nguenang, A.J. Kenfack, T.C. Kofané, Phys. Rev. E **66**, 56613 (2002)
25. J.P. Nguenang, T.C. Kofané, Physica D **147**, 311 (2000)
26. H.J. Mikeska, M. Steiner, Adv. Phys. **40**, 191 (1991)
27. L. Trallori, Phys. Rev. B **57**, 5923 (1998)
28. R.W. Wang, D.L. Mills, E.E. Fullerton, J.E. Mattson, S.D. Bader, Phys. Rev. Lett. **72**, 920 (1994)
29. E. De Lacheisserie, *Magnetostriction: Theory and applications* (CRC Press, USA, 1993)
30. G. Béranger, F. Duffault, J. Morlet, J.-F. Tiers, *Cent ans après la découverte de l'Invar . . . Les alliages de Fer et de Nickel: Technique et Documentation*, Paris (1996)
31. M. Remoissenet, M. Peyrard. J. Phys. C: Solid State. Phys. **14L**, 481 (1981)
32. M. Peyrard, M. Remoissenet, Phys. Rev. B **26**, 2886 (1982)
33. T.C. Kofané, J. Phys.: Condensed. Matter **11**, 2481 (1999)
34. A. Hubert, R. Schafer, Magnetic Domain (Springer-Verlag, Berlin, 2000), p. 288
35. H.J. Mikeska, E. Patzak, Z. Phys. B **26**, 253 (1977)
36. S. Roche, M. Peyrard, Phys. Lett. A **172**, 236 (1993)
37. G. Wysin, A.R. Bishop, P. Kumar, J. Phys. C: Solid. State. Phys. **15**, L337 (1982)
38. G. Wysin, A.R. Bishop, P. Kumar, J. Phys. C: Solid. State. Phys. **17**, 5975 (1984)
39. A.V. Savin, Y. Zolotaryuk, J.C. Eilbeck, Physica D **138**, 267 (2000)